

Mobility-controlled extremely large magnetoresistance in perfect electron-hole compensated α -WP₂ crystals

Yang-Yang Lv,¹ Xiao Li,² Jinglei Zhang,³ Bin Pang,¹ Si-Si Chen,² Lin Cao,¹ Bin-Bin Zhang,⁴ Dajun Lin,¹ Y. B. Chen,^{2,*} Shu-Hua Yao,^{1,†} Jian Zhou,¹ Shan-Tao Zhang,¹ Ming-Hui Lu,¹ Mingliang Tian,^{3,5} and Yan-Feng Chen^{1,5}

¹National Laboratory of Solid State Microstructures & Department of Materials Science and Engineering, Nanjing University, Nanjing 210093, China

²National Laboratory of Solid State Microstructures & Department of Physics, Nanjing University, Nanjing 210093, China

³Anhui Province Key Laboratory of Condensed Matter Physics at Extreme Conditions, High Magnetic Field Laboratory, Chinese Academy of Sciences, Hefei 230031, China

⁴Key Laboratory of Radiation Detection Materials and Devices, Ministry of Industry and Information Technology, School of Materials Science and Engineering & State Key Laboratory of Solidification Processing, Northwestern Polytechnical University, Xi'an 710072, China

⁵Collaborative Innovation Center of Advanced Microstructure, Nanjing University, Nanjing 210093, China



(Received 12 April 2018; revised manuscript received 11 June 2018; published 29 June 2018)

Recent studies discovered that the binary transition-metal compounds A_xB_y demonstrate extremely large magnetoresistance (XMR) under magnetic field B , for example, 10⁶% in PtBi₂ and 10⁵% in WTe₂. The underlying physical origins, however, are quite diverse, such as electron-hole balance, backscattering forbidden of Dirac/Weyl fermions, and high mobility. Here we experimentally find an ideal compound (α -WP₂) where the perfect electron-hole compensation can be sustained within a large temperature range (from 2 to 100 K). The XMR of α -WP₂ is measured as high as $8.74 \times 10^5\%$ under 9 T B at 2 K, but it is remarkably decreased from $8.74 \times 10^5\%$ to 18% when the temperature is raised from 2 to 100 K; simultaneously, the mobility is decreased by more than two orders of magnitude. Magnetotransport characterizations show that MR is proportional to B^2 and the pronounced dHvA quantum oscillations come from the conventional Schrödinger fermions in α -WP₂, which rules out the possibility of Dirac fermions. These evidences strongly suggest that XMR observed in binary A_xB_y semimetals is mainly attributed to high mobility, rather than Dirac/Weyl fermions, or resonant electron-hole compensation. This work elucidates the underlying physical origin of XMR in these compounds.

DOI: [10.1103/PhysRevB.97.245151](https://doi.org/10.1103/PhysRevB.97.245151)

I. INTRODUCTION

The binary transition-metal compounds A_xB_y , A normally being a transition/rare-earth metal and B oxygen/nitrogen group elements, have recently attracted much attentions by physics and materials communities, which are attributed to their two exciting physical properties. One is the observations of a series of topological quantum matters, for example, topological insulators [1–4], three-dimensional Dirac/Weyl semimetals (Na₃Bi [5], Cd₃As₂ [6], TX and TX₂ (T = Ta/Nb, X = As/P) [7–9]), type-II Weyl semimetals (W/MoTe₂ [10,11] and W/MoP₂ [12]), as well as Dirac nodal line state [13,14]. The other is the extremely large magnetoresistance (XMR) (e.g., Cd₃As₂ [15], Na₃Bi [16], W/MoTe₂ [17,18], LaSb and LaBi [19,20], PtBi₂ [21]), and sometimes large linear MR (Ag₂Te/Se [22,23]). The large MR observed in these materials do not come from magnetic properties (like giant MR in magnetic multilayer [24], colossal MR in manganese perovskite [25], and tunnel MR in magnetic tunnel junctions [26]), which should not be limited by magnetic domain size. But the physical origins leading to XMR in these binary compounds are quite diverse, such as linear energy dispersion at the quantum limit

[22,23], topological protection from backscattering mechanism [15], the resonant electron and hole compensation and high mobility [17,18,27], and the combination of compensated electron-hole pockets with a particular orbital texture [20]. Could we elucidate/unify the physical origin in these binary compounds?

Very recently we synthesized the transition-metal diphosphides α -Mo/WP₂ (space group $C2/m$) and β -Mo/WP₂ (space group $Cmc2_1$) [28]. The high temperature modification β phase, isostructural to MoP₂, is predicted to be a new candidate type-II topological Weyl semimetal [12]. Strikingly, we observed that there is the perfect electron-hole compensation sustained within a large temperature range (2 to 100 K) in α -WP₂. This compound provides an ideal system to elucidate the physical origin of XMR in binary A_xB_y .

In this article, detailed magnetotransport properties and de Haas–Van Alphen (dHvA) quantum oscillation of α -WP₂ have been systematically characterized. Crystal α -WP₂ exhibits extremely large and highly anisotropic XMR. Quantitatively, the unsaturated MR reaches $8.74 \times 10^5\%$ at 2 K under the magnetic field $B = 9$ T//[001] axis of an α -WP₂ crystal and electric field $E//b$ axis. Simultaneous fitting of Hall and MR data by a two-carrier model shows that the electron almost equals the hole carriers in the large temperature range (from 2 to 100 K), while the carrier mobility decreases rapidly when the temperature is raised from 2 to 100 K. At the same temperature

*ybchen@nju.edu.cn

†shyao@nju.edu.cn

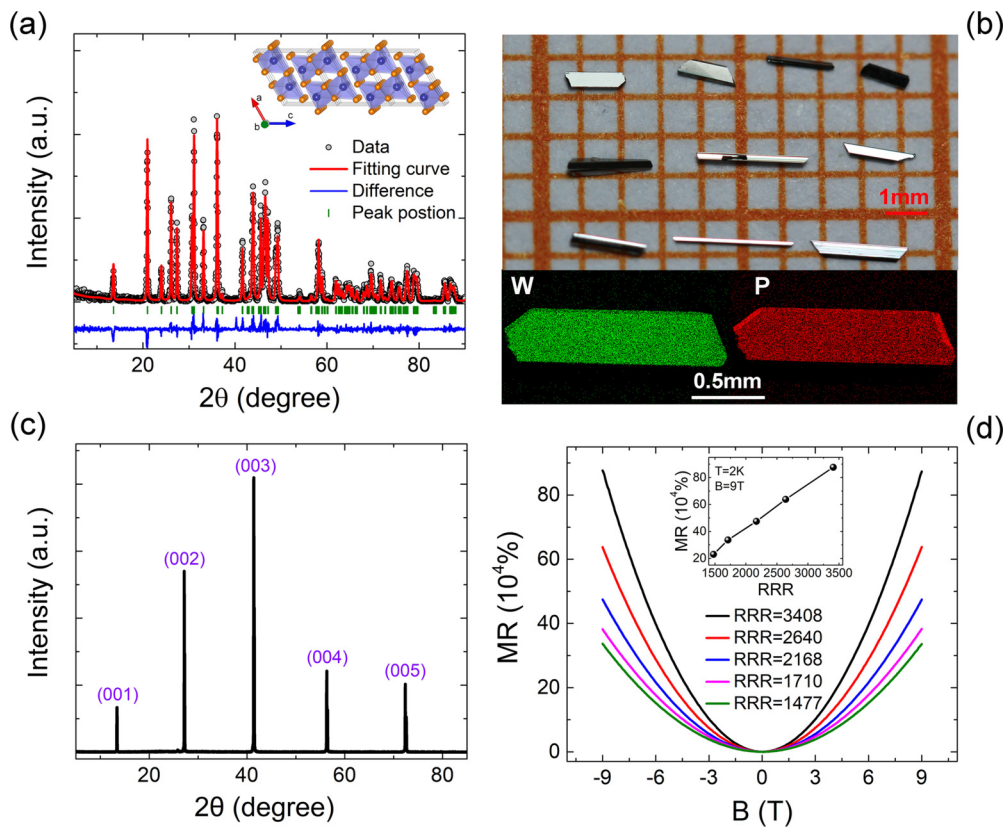


FIG. 1. (a) The Rietveld refinement of x-ray diffraction (XRD) data of polycrystalline α -WP₂ crystal measured at room temperature. Circle (°) marks and the red solid lines represent the experimental and Rietveld refinement results, respectively. The difference between the calculated and observed patterns is plotted at the bottom (blue line). The green vertical lines indicate the calculated positions of the Bragg reflections for the proposed crystal structure. The up inset is the crystal structure of α -WP₂. (b) The optical micrograph of as-grown α -WP₂ crystals and the energy-dispersive-spectroscopy (EDS) mapping image of W and P elements. (c) The XRD patterns of representative of α -WP₂ single crystals. (d) The magnetoresistance (MR) data of α -WP₂ single crystals with different RRR values at 2 K. The inset is the plot of MR vs RRR values. Crystal with the highest RRR exhibits the largest MR.

range, XMR decreases dramatically from $8.74 \times 10^5\%$ to 18%. It strongly suggests that the carrier mobility, rather than perfect electron-hole compensation, is decisive to the XMR effect in α -WP₂. Besides, pronounced dHvA quantum oscillations were observed at low temperatures and strongly dependent on the orientation of B . The dHvA analysis substantiates that there is no Dirac/Weyl fermions in α -WP₂. Magnetotransport behavior and dHvA are attributed to Fermiology of α -WP₂ predicted by the first-principles calculation under local density approximation.

II. MATERIALS AND METHODS

A. Sample growth and characterizations

High-quality single crystals of α -WP₂ were obtained by CVT using tellurium tetrabromide (TeBr₄) as a transport agent [29]. The growth procedure includes two steps. First, the polycrystalline powders were synthesized by the direct solid-state reaction using stoichiometric amounts of elemental W (Strem 99.999%) and P (Alfa Aesar 99.999%) in the sealed and evacuated ($P \sim 4 \times 10^{-6}$ Torr) quartz ampoule at about 650 °C for 5 days. Second, α -WP₂ polycrystals were mixed with 10 mg/ml of the transport agent TeBr₄ (Alfa Aesar 99.999%) and sealed in an evacuated quartz tube. Millimeter-

sized rodlike single crystals were successfully grown in a temperature gradient from 900 (source) to 800 °C (sink) for 10 days. To determine the crystal structure, powder x-ray diffraction (XRD) measurements of α -WP₂ polycrystals were performed using an Ultima III Rigaku x-ray diffractometer (Cu K_{α} radiation, $\lambda = 1.54056 \text{ \AA}$) with 2θ ranging from 5° to 90° at room temperature. The powder XRD results were analyzed by Rietveld refinement, using the general structure analysis software package GSAS-EXPGUI. The surface orientation and the stoichiometry of the polished crystals were confirmed by single-crystal XRD measurement and an energy dispersive spectroscopy (EDS) spectrometer in a FEI-Quanta scanning electron microscope (SEM) with internal calibration.

B. Transport measurements

A four-probe method was employed on the roughly rectangular crystals for the electrical transport measurements in a physical property measurement system (Quantum Design PPMS-9 T). The dHvA effect was detected by highly sensitive torque magnetometry methods which measure the magnetic susceptibility anisotropy of the crystal sample. The torque measurements were conducted on the Cell5 Water-Cooling

Magnet of high magnetic field up to 25 T at the High Magnetic Field Laboratory of the Chinese Academy of Sciences at Hefei.

C. The density functional theory (DFT) calculations

The band structure and Fermi surface of α -WP₂ are calculated by DFT in the generalized gradient approximation implemented in the Vienna *ab-initio* simulation package (VASP) code [30,31], in which the projected augmented wave method [32,33] and the Perdew-Burke-Ernzerhof exchange correlation are used [34]. The plane-wave cutoff energy of 350 eV and a k mesh of $13 \times 13 \times 9$ are used in the calculations. The lattice constants are taken from the refinement of our XRD data (see Table S1 [35]), but the atomic positions are optimized until the maximal residual forces on atoms are less than 0.01 eV/Å without spin-orbital coupling (SOC). We use a denser k mesh of $60 \times 60 \times 40$ in the Fermi surface calculation. SOC is included in all the calculations due to the large atom number of W.

III. RESULTS AND DISCUSSION

As illustrated in the inset of Fig. 1(a), each W atom is surrounded by six P atoms forming a trigonal prism with two additional P atoms outside the rectangular faces in α -WP₂. The prisms are stacked along the b axis through their trigonal faces to form the crystal frame. The powder XRD patterns and refinements of α -WP₂ are shown Fig. 1(a). Evidently, the calculated patterns (solid lines) agree very well with the experimental ones ($wR_p = 14.1\%$ and $R_p = 9.8\%$), confirming that the compounds crystallize in the monoclinic structures of the space group $C2/m$, which is consistent with previous reports [28,36,37]. The refined parameters are $a = 8.5039(2)$ Å, $b = 3.1694(1)$ Å, $c = 7.4649(2)$ Å, and $\beta = 119.3354(1)^\circ$. Figure 1(b) shows the typical photograph of the as-grown α -WP₂ single crystals and the EDS mappings of W and P elements. The W and P elements are uniformly distributed in the sample. Quantitative EDS analysis indicates that the ratio between W and P is 1:1.995, which is quite close to the stoichiometric formula. The XRD pattern of α -WP₂ single crystal is presented in Fig. 1(c). When the x-ray beam was incident perpendicular to the surface, only reflections of $(00l)$ planes can be detected, which reveals the exposed surface of crystals being ab plane. In addition, the full width at half maximum of the (001) pole is as small as 0.07° , substantiating the high crystalline quality of grown α -WP₂. Figure 1(d) plots the comparison of the MR ($MR = [\rho(B) - \rho_0]/\rho_0$, where ρ_0 is the resistance without B), measured at 9 T and 2 K, of different crystals with various residual resistivity ratio (RRR) [$RRR = \rho_{(300K)}/\rho_{(2K)}$] synthesized in our lab. The electric current is parallel to the b axis, and the magnetic field is perpendicular to the ab plane. We find that the RRR of our α -WP₂ crystals ranging from 1400 to 3500 and the values of MR reduce gradually with decreased RRR values. In general, the high RRR value is a good indicator of excellent crystal quality. The result indicates that the crystal quality is very crucial to characterize the intrinsic physical properties. So, we choose the sample with a higher RRR value (~ 3408) to investigate its intrinsic magnetotransport properties. Quantitatively, this sample exhibits a large longitudinal MR of $8.74 \times 10^5\%$ [shown in Fig. 1(d)] at 2 K and 9 T.

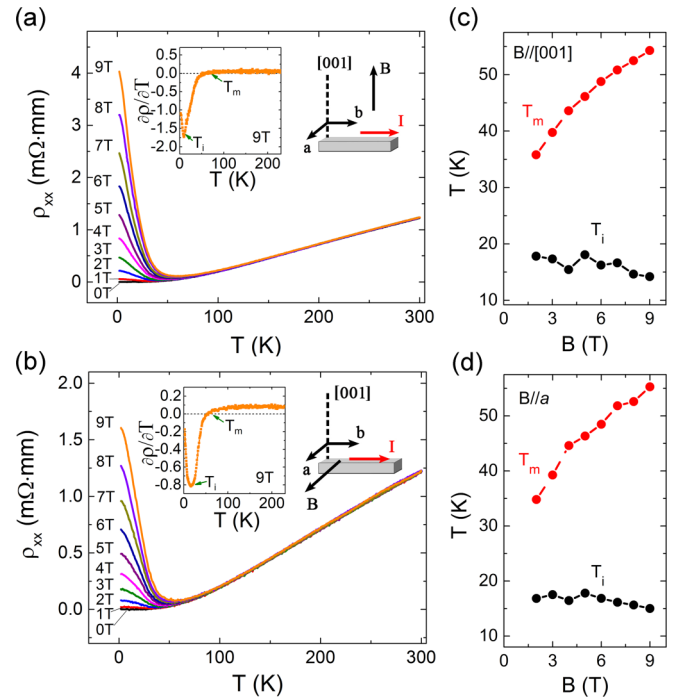


FIG. 2. (a) and (b) Temperature-dependent resistivities of ρ_{xx} for α -WP₂ single crystals at various magnetic fields B in a temperature range of 2–300 K with the electric current I along the b axis for the $B//[001]$ axis and $B//a$ axis, respectively. The upper-right inset is the schematic of the experiment. The upper-left inset is $\partial\rho/\partial T$ as a function of temperature. Two transition temperatures are indicated as T_m and T_i . T_m labels the temperature with minimum resistivity; T_i does temperature with minimum temperature-differentiated resistivity. (c) and (d) The magnetic field dependence of T_m and T_i for the $B//[001]$ axis (I) and $B//a$ axis (II), respectively.

We measured the temperature dependence of the resistivity ρ_{xx} with $B//[001]$ and $B//a$ direction, and the electric current I along the b axis, as shown in Figs. 2(a) and 2(b), respectively. It is noted that in both configurations, B is always perpendicular to I . The ρ_{xx} - T curves for the α -WP₂ sample shown here are reproducible by checking several crystals synthesized under the same growth condition. At the zero field, ρ_{xx} exhibits a metallic behavior. Quantitatively, ρ_{xx} are 1.22×10^{-4} and 3.58×10^{-8} Ω cm at 300 and 2 K, respectively, showing the quite high RRR ~ 3408 . With the application of the perpendicular B , ρ_{xx} first decreases and then increases rapidly upon cooling, indicating that α -WP₂ may undergo a magnetic-field-induced metal-semiconductorlike transition (MST) [38,39]. Here the term “semiconductorlike” just emphasizes that temperature-differentiated resistance is negative in low T and high B regimes ($d\rho/dT < 0$), which is the feature of semiconductors. To get in-depth understanding of the exotic transport behavior, we plotted the derivative $\partial\rho_{xx}/\partial T$ curves at 9 T in the insets of Figs. 2(a) and 2(b), respectively, where T_m and T_i are determined as the sign change point and the minimum in the $\partial\rho_{xx}/\partial T$ curve. Based on the field dependence of $\partial\rho_{xx}/\partial T$ curves under different B , the B -dependent T_m and T_i are plotted in Figs. 2(c) and 2(d). The field-induced MST has been observed in other compounds demonstrating XMR too [20]. Obviously, T_m increases rapidly with the increase

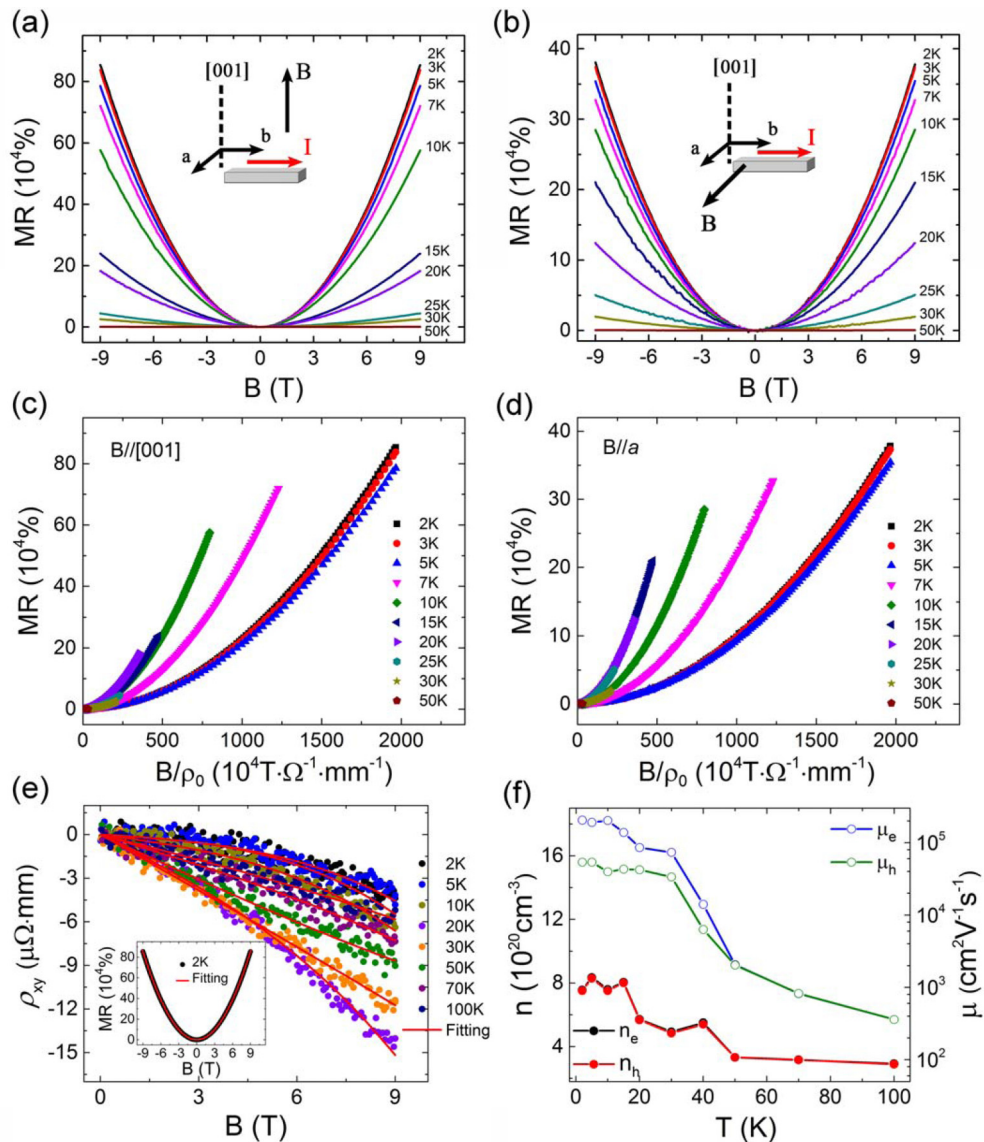


FIG. 3. (a) and (b) The magnetic field dependence of MR for α -WP₂ single crystals at various temperatures with $I \parallel b$ axis for the $B \parallel [001]$ axis and $B \parallel a$ axis, respectively. (c) and (d) Kohler's plot of α -WP₂ MR data from 2 to 50 K using $MR = F(B/\rho_0)$ with two different magnetic field directions: $[001]$ axis and a axis, respectively. (e) Hall resistivity ρ_{xy} as functions of $B \parallel [001]$ axis for a α -WP₂ single crystal and for temperatures ranging from 2 to 100 K. Red lines are fitting results by the two-band model. The inset is the MR of the α -WP₂ single crystal measured at 2 K and its fitting by the two-band model. (f) The dependence of charge carrier densities n_e and n_h , as well as carrier mobility μ_e and μ_h of electrons and holes on temperature, respectively. These values were extracted from fitting by the two-carrier model.

of B and T_i remains almost unchanged even at high fields for both configurations $B \parallel [001]$ axis and $B \parallel a$ axis. The physical origin of MST in α -WP₂ is out of the scope of this article. Currently, the physical origin of MST observed in these semimetals is attributed to decreased carrier concentration [20] or decreased mobility under large B [40]. We believe that these two mechanisms cannot be distinguished just by transport data because the conductivity is the product of carrier concentration and mobility.

Figures 3(a) and 3(b) show the B dependence of MR at various temperatures for $B \parallel [001]$ and a axis with keeping B perpendicular to I , respectively. At low temperature, the sample shows nonsaturating XMR effect, which reaches $8.74 \times 10^5\%$ for the $B \parallel [001]$ axis and $3.81 \times 10^5\%$ for the $B \parallel a$ axis at

2 K and 9 T. MR is suppressed significantly with increasing temperature, and becomes negligibly small above 100 K. We also find that the MR data at 2 K are well described by a nearby quadratic field dependence $MR \propto B^{1.95}$ ($B \parallel [001]$ axis) and $MR \propto B^{1.97}$ ($B \parallel a$ axis), up to the maximum field (9 T).

According to semiclassical transport theory, the well-known Kohler's rule claims that the MR follows a scaling function of B/ρ_0 [$MR = F(B/\rho_0)$] in a metal of a single type of charge carrier or single scattering mechanism [41], where ρ_0 is the zero-field resistivity at the certain temperature. Based on Kohler's rule, the plots of MR as a function of B/ρ at different temperatures will collapse onto a single curve. As plotted in Figs. 3(c) and 3(d), the MR in α -WP₂ obviously deviates from Kohler's rule above 5 K and this violation is

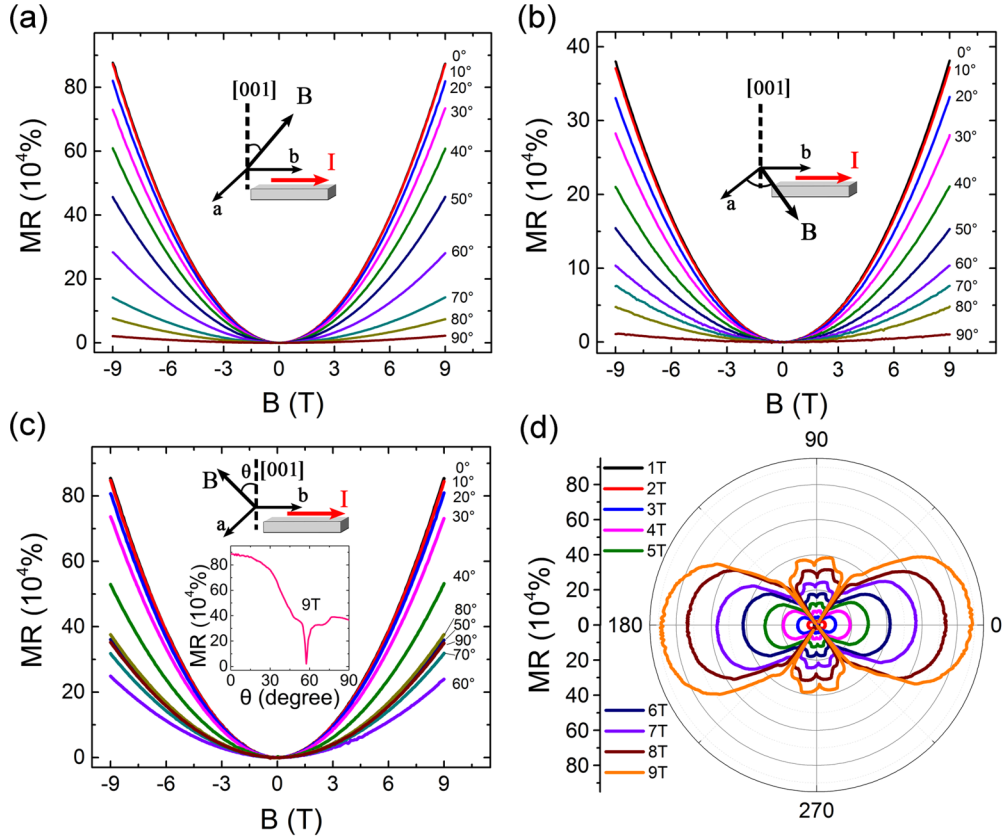


FIG. 4. (a) The magnetic field dependence of MR measured at 2 K for α -WP₂ single crystals with $I \parallel b$ axis and the magnetic field rotating from the [001] axis ($\theta = 0^\circ$) to the b axis (90°). Inset is the schematic of the experiment. (b) The magnetic field dependence of MR measured at 2 K at different angles in the ab plane with the $I \parallel b$ axis. (c) The magnetic field dependence of MR measured at 2 K with the $I \parallel b$ axis and the B is tilted from the [001] axis (0°) to the a axis (90°). Upper inset is the schematic of the experiment. Bottom inset is the angle-dependent MR curve measured under 9 T magnetic field. (d) The polar diagram of the angle-dependent MR measured under 2 K and 9 T, B was rotated in the ac plane.

common in some XMR materials [42,43], which may originate from multiband electrical carriers at low temperature, or the existence of multiple scattering mechanisms emerging at high temperature [41]. This conclusion also can be reached using the generalized Kohler's plot [44]. Combining the B^2 -dependent MR and violation of Kohler's rule, it can be concluded that there is perfect electron-hole compensation in α -WP₂.

In order to extract the detailed information of charge carrier, we also performed the measurements of Hall resistivity on the α -WP₂ single crystal for the B applied along the [001] axis and different temperatures between 2 and 100 K [see Fig. 3(e)]. Obviously the Hall resistivities show nonlinear behavior at low fields, which is the evidence for the coexistence of both electron and hole. The classical two-band model was successfully adopted to fit the MR [Eq. (1)] and Hall data [Eq. (2)] [45]:

$$\rho_{xx} = \frac{1}{e} \frac{(n_h \mu_h + n_e \mu_e) + (n_h \mu_e + n_e \mu_h) \mu_h \mu_e B^2}{(n_h \mu_h + n_e \mu_e)^2 + (n_h - n_e)^2 \mu_h^2 \mu_e^2 B^2}, \quad (1)$$

$$\rho_{yx} = \frac{B}{e} \frac{(n_h \mu_h^2 - n_e \mu_e^2) + (n_h - n_e) \mu_h^2 \mu_e^2 B^2}{(n_h \mu_h + n_e \mu_e)^2 + (n_h - n_e)^2 \mu_h^2 \mu_e^2 B^2}, \quad (2)$$

where n_e (or n_h) and μ_e (or μ_h) are the density of electrons (or holes) and the mobility of electrons (or holes),

respectively. The temperature-dependent carrier concentrations and mobilities are displayed in Fig. 3(f). Evidently, n_h almost equals n_e from 2 to 100 K ($n_e = 7.55 \times 10^{20} \text{ cm}^{-3}$ and $n_h = 7.51 \times 10^{20} \text{ cm}^{-3}$ at 2 K), confirm that α -WP₂ is a perfect compensated semimetal, and all the carrier densities decrease with temperature increased. The mobilities of the electron and hole decrease rapidly when the temperature is increased from 2 to 100 K ($\mu_e = 2.04 \times 10^5 \text{ cm}^2 \text{ V}^{-1} \text{ s}^{-1}$ and $\mu_h = 5.36 \times 10^4 \text{ cm}^2 \text{ V}^{-1} \text{ s}^{-1}$ at 2 K, $\mu_e = \mu_h = 3.58 \times 10^2 \text{ cm}^2 \text{ V}^{-1} \text{ s}^{-1}$ at 100 K). It should be mentioned that to avoid the numerical arbitrary in fitting by four parameters in the two-band model, the hole/electron concentrations are constrained by those extracted by the quantum oscillation analysis described below. This result strongly suggests that the carrier mobility is decisive to the large MR effect of α -WP₂. The decreased mobility at high temperature can be expected because electron-phonon scattering is dramatically increased at high temperature.

To further explore the MR behavior of α -WP₂, we studied the angle-dependent MR behavior at 2 K under different measurement configurations. Figure 4 shows the MR when B is tilted in different directions while the I is always aligned along b direction. In order to avoid the current jetting effect, the sample was chosen to be regular shape with four electrodes

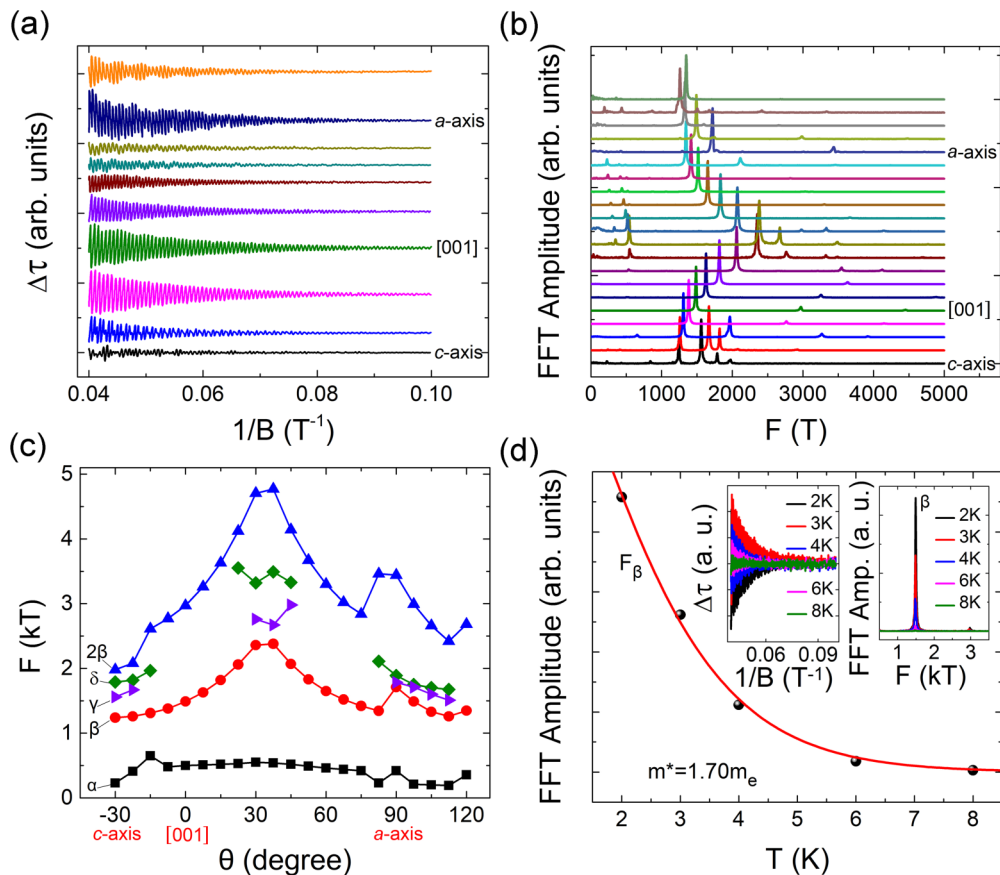


FIG. 5. (a) The dHvA oscillations as a function of $1/B$ after subtracting background with the B rotated in the ac plane. (b) The corresponding FFT spectra of the angular-dependent dHvA oscillations. (c) The angular dependence of the dHvA oscillation frequency. (d) The temperature dependence of oscillating amplitude for the main frequencies F_β . Red solid line is fitted by the Lifshitz-Kosevich formula. The left inset is the oscillatory components obtained by subtracting background at different temperatures. The right inset is the FFT spectra for the F_β mode dHvA oscillation at different temperatures.

fully crossing the width in this measurement [41]. As shown in Fig. 4(a), when the B is tilted from [001] direction to b axis, the MR drops monotonically and rapidly. Similar MR behavior was observed by tilting B from a to b axis, as presented in Fig. 4(b). Figure 4(c) shows the MR with B tilted from the [001] direction to the a axis. Two remarkable features can be observed, one is that MR is dependent on B^2 , no matter which direction the B is aligned (see Fig. S2 in the Supplemental Material [35]), which strongly suggests the perfect electron-hole compensation in α -WP₂ crystal. This is different from the normal scenario that MR will be saturated at high B [41]. The other is that the MR decreases nonmonotonically with the misaligned angle between B and [001], reduces to $2.40 \times 10^5\%$ under the misaligned angle about 60° , and decreases about two orders of magnitude when the misaligned angle is about 57.5° [see inset of Fig. 4(c)]. To demonstrate the anisotropic MR clearly, Fig. 4(d) displays the polar diagram of the angle-dependent MR at 2 K with different magnetic field B rotated in the ac plane perpendicular to the crystallographic b axis. Clearly the α -WP₂ sample exhibits a significantly anisotropic MR behavior with a butterflylike pattern under different magnetic field B . This extremely anisotropic MR observed in α -WP₂, quite promising to magnetic sensor devices, is originated from the open orbitals at the Fermi surface discussed as follows.

Quantum oscillation is a powerful tool to investigate the Fermi surface of the given material [46]. We measured de Haas-van Alphen (dHvA) oscillations in α -WP₂ at different temperatures with the B rotated in the ac plane. As shown in Fig. 5(a), after the background subtraction, the oscillation patterns of $\Delta\tau$ display a clear evolution with the tilting of B . The corresponding fast Fourier transform (FFT) spectra of dHvA are presented in Fig. 5(b) indicating that multiple frequencies are derived from the oscillations. For the dHvA measurement under the $B//[001]$ axis, three main frequencies are observed: 500, 1490, and 2970 T, marked as F_α , F_β , and $F_{2\beta}$, respectively. And some rather small frequencies may result from artifacts in numerical fast Fourier transformation. The positions of these FFT peaks vs the B direction are summarized in Fig. 5(c). As the B was tilted to the crystallographic a axis in the ac plane, F_α remains at about 500 T which is independent on tilting angle; while F_β and $F_{2\beta}$ increase with the misaligned angle (θ) increasing from 0° to 30° , then reaching a maximum 2360 and 4704 T at θ around 30° , after that decreasing with θ increasing. In addition, two more frequencies ($F_\gamma \approx 1560$ T and $F_\delta \approx 1790$ T) appear when the $B//c$ axis ($\theta \sim -30^\circ$) and their evolution trends are quite similar to F_β and $F_{2\beta}$. The left inset of Fig. 5(d) displays the oscillatory components as a function of $1/B$ at different temperatures

under the $B//[001]$ axis. The oscillation of the F_β mode dampens quickly with temperature increased and disappears above 8 K (F_α oscillation cannot be distinguished at 4 K), indicating a heavy cyclotron mass/low mobility in α -WP₂. The corresponding FFT spectra at different temperatures are shown in the right inset of Fig. 5(d). In order to obtain the effective mass for the main frequencies F_β , we fit the temperature-dependent FFT amplitude using the Lifshitz-Kosevich formula [46]:

$$A \propto \frac{2\pi^2 k_B T m^* / e B_i \hbar}{\sinh(2\pi^2 k_B T m^* / e B_i \hbar)} = \frac{\alpha m^* T / B_i}{\sinh(\alpha m^* T / B_i)}, \quad (3)$$

where $\alpha = 2\pi k_B / e \hbar$ is a constant (about 14.69 T K⁻¹), $m^* = m/m_e$ is the effective mass (m_e is the mass of free electron), and B_i is determined by the frequency of i oscillation. The fitting result is shown in Fig. 5(d) and the cyclotron mass for the main frequency F_β is estimated to be 1.70 m_e . The effective mass comparable to m_e , as well as the intercept in Landau fan diagram as 0.12 closing to the 3D Schrödinger fermion [35,46], suggest the quantum oscillation of α -WP₂ coming from the conventional Schrödinger electron, rather than Dirac/Weyl fermion.

At the following parts, we tried to correlate the observed extremely large and highly anisotropic MR, as well as dHvA to the topology of the Fermi surface calculated by the first-principles calculation. Figure 6 shows the electronic band structure and Fermi surface of stoichiometric α -WP₂. Evidently there are three features in α -WP₂: (1) there are both electron and hole coexistence on the Fermi level; (2) the hole pockets include a small ellipsoid and an open orbital that are labeled by two white arrows; and (3) there are only closed pockets for the electron. This electron pocket likes a big chunk connected by two droplets which are highlighted by three ellipses [see Fig. 6(c)]. Based on these features, the observed extremely anisotropic MR, as well as dHvA oscillations of α -WP₂, can be rationalized. First, the unsaturated MR of α -WP₂, as well as an approximate quadratic- B dependent MR, can be naturally understood, which is attributed to perfect electron-hole compensation as predicted by a classical two-carrier model [41]. Similar MR behavior is also observed in WTe₂ crystals [17]. The extremely anisotropic MR shown in the inset of Fig. 4(c), observed under B tilted from $[001]$ to a direction and the current I applied along b direction at low temperature, can be attributed to the open orbital of the hole pocket. The minimum MR is observed when the misaligned angle between B and $[001]$ is about 57.5°, B is nearly perpendicular to the open orbital. In this condition, the orientations between B and current I with respect to the open orbital are shown in Fig. 6(b) too. Evidently, the limitation of Fermi surface topology makes the holes moving along b direction directly rather than cyclotron movement in the closed orbital, which effectively enhances the conductivity [41].

Finally, we would like to assign the observed dHvA frequencies of α -WP₂ to the specific electron/hole pockets. Obviously there is a spherelike hole pocket that leads to dHvA oscillation F_α . Conceptually, frequency of dHvA oscillation in a sphere is in-dependent on the tilting angle [46], which is in agreement to observation [see Fig. 5(c)]. Quantitatively, the maximum cross

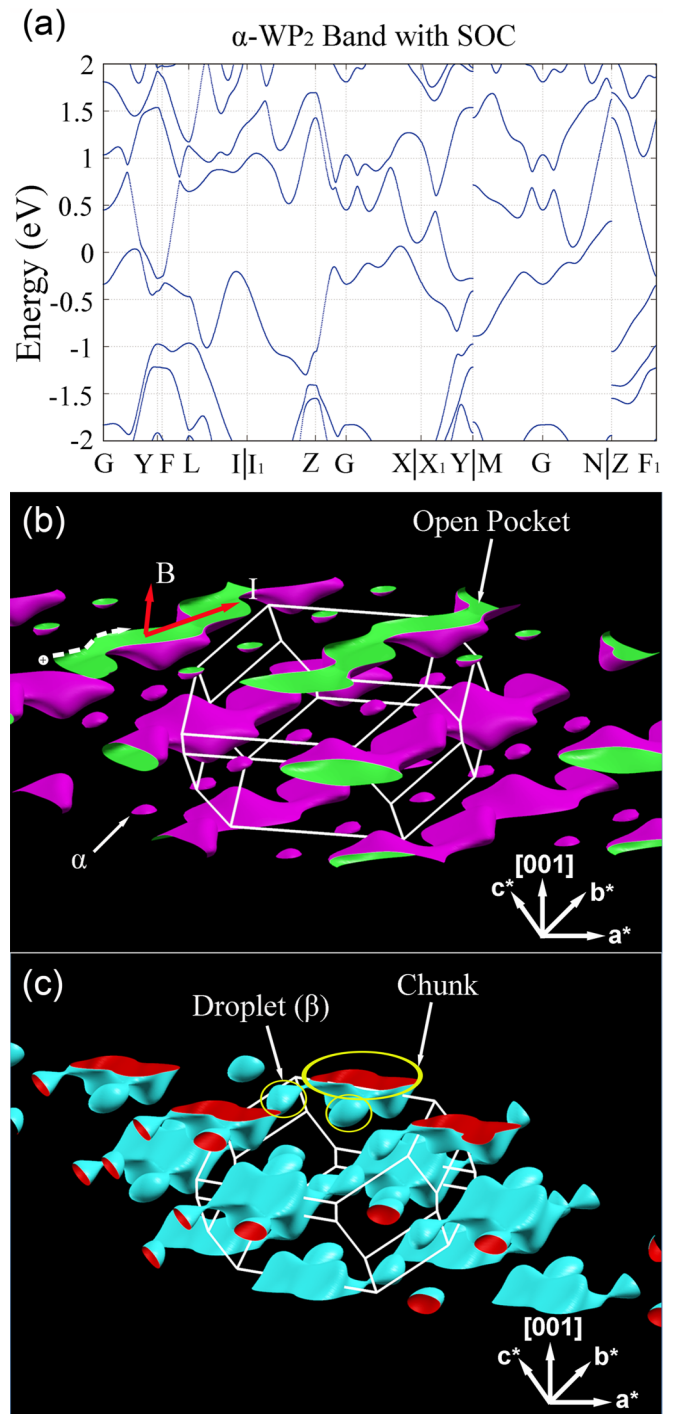


FIG. 6. (a) The band structures of α -WP₂. (b) The hole Fermi surfaces. A spherelike pocket (α pocket) and open orbital are highlighted by white arrows. α pocket leads to the F_α frequency measured in the dHvA oscillation. The configuration of B and current I on an open orbital leading to the MR minimum shown in Fig. 4(c) is schematically drawn by red arrows (top-left schematic). (c) The electron Fermi surfaces. Two droplets connect slightly to a big chunk. Two droplets (β pocket) and a big chunk are indicated by three yellow ellipses. The F_β frequency measured in the dHvA oscillation may come from the β pocket. To see whole features of Fermi surfaces, eight Brillouin zones are drawn in (b) and (c).

section of this pocket can be measured as 0.015 \AA^{-2} , which is quite close to the experimental value (0.02 \AA^{-2}). Therefore, F_α can be unambiguously assigned to the hole-pocket α . The dHvA frequency of F_β is tentatively attributed to the electron pocket β [dropletlike pocket in Fig. 6(c)], which is slightly connected to a big chunk. Quantitatively, the maximum cross section of the electron pocket β can be measured as 0.08 \AA^{-2} . This value is also quite close to the experimental value ($\approx 0.12 \text{ \AA}^{-2}$), which suggests our assignment of dHvA frequency F_β might be reasonable. It should be mentioned that F_γ and F_δ , observed when B is tilted to the c axis, might come from the same electron pocket leading to F_β too. This is because the frequencies of these oscillations are quite close and have similar tilting-angle dependence [see Fig. 5(c)].

The above-discussed comparison between MR/dHvA oscillation and theoretical Fermi surface suggests that the electronic band structure of α -WP₂ calculated by first-principles calculation is physically reasonable. Certainly the whole features of Fermi surface α -WP₂ should be double checked by angle-resolved photoemission spectroscopy.

IV. CONCLUSIONS

In conclusion, highly crystalline α -WP₂ crystals have been successfully synthesized by the chemical vapor transport (CVT) method. Under the external magnetic field, temperature-dependent resistivity shows the metal-semiconductorlike transition. Magnetoresistance is nonsaturated and parabolically dependent on B , and reached as high

as $8.74 \times 10^5\%$ for the $B//[001]$ axis under 9 T at 2 K. Simultaneous fitting of Hall and MR data by the two-carrier model shows that the electron almost equals the hole carriers in the large temperature range (2–100 K), while the carrier mobility decreases in magnitude when the temperature is raised from 2 to 100 K. Meanwhile, XMR decreases dramatically from $8.74 \times 10^5\%$ to 18%. The measured magnetotransports and dHvA oscillation can be rationalized by the theoretical Fermi surface of α -WP₂, and it rules out the existence of Dirac/Weyl fermions therein. These systematical analyses strongly suggest that the carrier mobility, rather than perfect electron-hole compensation, backscattering forbidden of Dirac/Weyl fermions, is decisive to the XMR effect in α -WP₂. Considering the crystal- and electronic-structure similarity between many A_xB_y and α -WP₂, the crucial factor leading to measured XMR therein should be carrier mobility.

ACKNOWLEDGMENTS

We would like to acknowledge the financial support from the State Key Program for Basic Research of China (973 Program) (2015CB921203 and 2015CB659400), the National Natural Science Foundation of China (51472112, 11574131, 11374149, 11474150, and 9162212), the Natural Science Foundation of Jiangsu Province, China (BK20171343), the Foundation for Innovative Research Groups of the National Natural Science Foundation of China (51721001), and the National Key R&D Program of China (2016YFA0201104). Yang-Yang Lv acknowledges the financial support from the program A for Outstanding Ph.D. candidate of Nanjing University (201701A008).

-
- [1] M. König, S. Wiedmann, C. Brüne, A. Roth, H. Buhmann, L. W. Molenkamp, X.-L. Qi, and S.-C. Zhang, Quantum spin hall insulator state in HgTe quantum wells, *Science* **318**, 766 (2007).
 - [2] W. Zhang, R. Yu, W. X. Feng, Y. G. Yao, H. M. Weng, X. Dai, and Z. Fang, Topological Aspect and Quantum Magnetoresistance of β -Ag₂Te, *Phys. Rev. Lett.* **106**, 156808 (2011).
 - [3] H. M. Weng, X. Dai, and Z. Fang, Transition-Metal Pentatelluride ZrTe₅ and HfTe₅: A Paradigm for Large-Gap Quantum Spin Hall Insulators, *Phys. Rev. X* **4**, 011002 (2014).
 - [4] X. F. Qian, J. W. Liu, L. Fu, and J. Li, Quantum spin Hall effect in two-dimensional transition metal dichalcogenides, *Science* **346**, 1344 (2014).
 - [5] Z. J. Wang, Y. Sun, X.-Q. Chen, C. Franchini, G. Xu, H. M. Weng, X. Dai, and Z. Fang, Dirac semimetal and topological phase transitions in A₃Bi (A = Na, K, Rb), *Phys. Rev. B* **85**, 195320 (2012).
 - [6] Z. J. Wang, H. M. Weng, Q. S. Wu, X. Dai, and Z. Fang, Three-dimensional Dirac semimetal and quantum transport in Cd₃As₂, *Phys. Rev. B* **88**, 125427 (2013).
 - [7] H. Weng, C. Fang, Z. Fang, B. A. Bernevig, and X. Dai, Weyl Semimetal Phase in Noncentrosymmetric Transition-Metal Monophosphides, *Phys. Rev. X* **5**, 011029 (2015).
 - [8] S.-M. Huang, S.-Y. Xu, I. Belopolski, C.-C. Lee, G. Chang, B. K. Wang, N. Alidoust, G. Bian, M. Neupane, C. Zhang, S. Jia, A. Bansil, H. Lin, and M. Z. Hasan, A Weyl Fermion semimetal with surface Fermi arcs in the transition metal monpnictide TaAs class, *Nat. Commun.* **6**, 7373 (2015).
 - [9] D. Gresch, Q. S. Wu, G. W. Winkler, and A. A. Soluyanov, Hidden Weyl points in centrosymmetric paramagnetic metals, *New J. Phys.* **19**, 035001 (2017).
 - [10] A. A. Soluyanov, D. Gresch, Z. J. Wang, Q. S. Wu, M. Troyer, X. Dai, and B. A. Bernevig, Type-II Weyl semimetals, *Nature (London)* **527**, 495 (2015).
 - [11] Y. Sun, S.-C. Wu, M. N. Ali, C. Felser, and B. H. Yan, Prediction of Weyl semimetal in orthorhombic MoTe₂, *Phys. Rev. B* **92**, 161107(R) (2015).
 - [12] G. Autès, D. Gresch, M. Troyer, A. A. Soluyanov, and O. V. Yazyev, Robust Type-II Weyl Semimetal Phase in Transition Metal Diphosphides XP₂ (X = Mo, W), *Phys. Rev. Lett.* **117**, 066402 (2016).
 - [13] J. L. Lu, W. Luo, X. Y. Li, S. Q. Yang, J. X. Cao, X. G. Gong, and H. J. Xiang, Two-dimensional node-line semimetals in a honeycomb-kagome lattice, *Chin. Phys. Lett.* **34**, 057302 (2017).
 - [14] Y.-J. Jin, R. Wang, J.-Z. Zhao, Y.-P. Du, C.-D. Zheng, L.-Y. Gan, J.-F. Liu, H. Xu, and S. Y. Tong, The prediction of a family group of two-dimensional node-line semimetals, *Nanoscale* **9**, 13112 (2017).
 - [15] T. Liang, Q. Gibson, M. N. Ali, M. Liu, R. J. Cava, and N. P. Ong, Ultrahigh mobility and giant magnetoresistance in the Dirac semimetal Cd₃As₂, *Nat. Mater.* **14**, 280 (2015).

- [16] J. Xiong, S. K. Kushwaha, T. Liang, J. W. Krizan, M. Hirschberger, W. Wang, R. J. Cava, and N. P. Ong, Evidence for the chiral anomaly in the Dirac semimetal Na_3Bi , *Science* **350**, 413 (2015).
- [17] M. N. Ali, J. Xiong, S. Flynn, J. Tao, Q. D. Gibson, L. M. Schoop, T. Liang, N. Haldolaarachchige, M. Hirschberger, N. P. Ong, and R. J. Cava, Large, non-saturating magnetoresistance in WTe_2 , *Nature (London)* **514**, 205 (2014).
- [18] D. H. Keum, S. Cho, J. H. Kim, D.-H. Choe, H.-J. Sung, M. Kan, H. Kang, J.-Y. Hwang, S. W. Kim, H. Yang, K. J. Chang, and Y. H. Lee, Bandgap opening in few-layered monoclinic MoTe_2 , *Nat. Phys.* **11**, 482 (2015).
- [19] F. F. Tafti, Q. D. Gibson, S. K. Kushwaha, N. Haldolaarachchige, and R. J. Cava, Resistivity plateau and extreme magnetoresistance in LaSb , *Nat. Phys.* **12**, 272 (2016).
- [20] F. F. Tafti, Q. Gibson, S. Kushwaha, J. W. Krizan, N. Haldolaarachchige, and R. J. Cava, Temperature-field phase diagram of extreme magnetoresistance, *Proc. Natl. Acad. Sci. USA* **113**, E3475 (2016).
- [21] W. S. Gao, N. N. Hao, F.-W. Zheng, W. Ning, M. Wu, X. D. Zhu, G. L. Zheng, J. L. Zhang, J. W. Lu, H. W. Zhang, C. Y. Xi, J. Y. Yang, H. F. Du, P. Zhang, Y. H. Zhang, and M. L. Tian, Extremely Large Magnetoresistance in a Topological Semimetal Candidate Pyrite PtBi_2 , *Phys. Rev. Lett.* **118**, 256601 (2017).
- [22] R. Xu, A. Husmann, T. F. Rosenbaum, M.-L. Saboungi, J. E. Enderby, and P. B. Littlewood, Large magnetoresistance in non-magnetic silver chalcogenides, *Nature (London)* **390**, 57 (1997).
- [23] C.-L. Zhang, F. Schindler, H. W. Liu, T.-R. Chang, S.-Y. Xu, G. Q. Chang, W. Hua, H. Jiang, Z. J. Yuan, J. L. Sun, H.-T. Jeng, H.-Z. Lu, H. Lin, M. Z. Hasan, X. C. Xie, T. Neupert, and S. Jia, Electron scattering in tantalum monoarsenide, *Phys. Rev. B* **96**, 165148 (2017).
- [24] M. N. Baibich, J. M. Broto, A. Fert, F. Nguyen Van Dau, F. Petroff, P. Etienne, G. Creuzet, A. Friederich, and J. Chazelas, Giant Magnetoresistance of (001)Fe/(001)Cr Magnetic Superlattices, *Phys. Rev. Lett.* **61**, 2472 (1988).
- [25] Y. Moritomo, A. Asamitsu, H. Kuwahara, and Y. Tokura, Giant magnetoresistance of manganese oxides with a layered perovskite structure, *Nature (London)* **380**, 141 (1996).
- [26] T. Miyazaki and N. Tezuka, Spin polarized tunneling in ferromagnet/insulator/ferromagnet junctions, *J. Magn. Magn. Mater.* **151**, 403 (1995).
- [27] Y.-Y. Lv, B.-B. Zhang, X. Li, B. Pang, F. Zhang, D.-J. Lin, J. Zhou, S.-H. Yao, Y. B. Chen, S.-T. Zhang, M. H. Lu, Z. K. Liu, Y. L. Chen, and Y.-F. Chen, Dramatically decreased magnetoresistance in nonstoichiometric WTe_2 crystals, *Sci. Rep.* **6**, 26903 (2016).
- [28] M. Y. Pi, T. L. Wu, D. K. Zhang, S. J. Chen, and S. X. Wang, Phase-controlled synthesis and comparative study of α - and β - WP_2 submicron particles as efficient electrocatalysts for hydrogen evolution, *Electrochim. Acta* **216**, 304 (2016).
- [29] Y.-Y. Lv, B.-B. Zhang, X. Li, S.-H. Yao, Y. B. Chen, J. Zhou, S.-T. Zhang, M.-H. Lu, and Y.-F. Chen, Extremely large and significantly anisotropic magnetoresistance in ZrSiS single crystals, *Appl. Phys. Lett.* **108**, 244101 (2016).
- [30] G. Kresse and J. Hafner, *Ab initio* molecular dynamics for open-shell transition metals, *Phys. Rev. B* **48**, 13115 (1993).
- [31] G. Kresse and J. Furthmüller, Efficiency of ab-initio total energy calculations for metals and semiconductors using a plane-wave basis set, *Comput. Mater. Sci.* **6**, 15 (1996).
- [32] P. E. Blöchl, Projector augmented-wave method, *Phys. Rev. B* **50**, 17953 (1994).
- [33] G. Kresse and D. Joubert, From ultrasoft pseudopotentials to the projector augmented-wave method, *Phys. Rev. B* **59**, 1758 (1999).
- [34] J. P. Perdew, K. Burke, and M. Ernzerhof, Generalized Gradient Approximation Made Simple, *Phys. Rev. Lett.* **77**, 3865 (1996).
- [35] See Supplemental Material at <http://link.aps.org/supplemental/10.1103/PhysRevB.97.245151> for the crystal structural parameters of as-grown α - WP_2 crystals, the dHvA oscillations of as-grown α - WP_2 crystals measured at 2 K with the B along the [001]-axis, the fitting data a and n of the MR at 2 K under different experiment configurations with power law $\text{MR} = a \times B^n$, and Landau-fan diagram analysis of quantum oscillations in α - WP_2 crystals.
- [36] F. Hulliger, New representatives of the NbAs_2 and ZrAs_2 structures, *Nature (London)* **204**, 775 (1964).
- [37] H. Mathis, R. Glaum, and R. Gruehn, Reduction of WO_3 by phosphorus, *Acta Chem. Scand.* **45**, 781 (1991).
- [38] X. Du, S. W. Tsai, D. L. Maslov, and A. F. Hebard, Metal-Insulator-Like Behavior in Semimetallic Bismuth and Graphite, *Phys. Rev. Lett.* **94**, 166601 (2005).
- [39] D. V. Khveshchenko, Magnetic-Field-Induced Insulating Behavior in Highly Oriented Pyrolytic Graphite, *Phys. Rev. Lett.* **87**, 206401 (2001).
- [40] A. Narayanan, M. D. Watson, S. F. Blake, N. Bruyant, L. Drigo, Y. L. Chen, D. Prabhakaran, B. Yan, C. Felser, T. Kong, P. C. Canfield, and A. I. Coldea, Linear Magnetoresistance Caused by Mobility Fluctuations in n -Doped Cd_3As_2 , *Phys. Rev. Lett.* **114**, 117201 (2015).
- [41] A. B. Pippard, *Magnetoresistance in Metals* (Cambridge University Press, Cambridge, 1989).
- [42] A. F. Wang, D. Graf, A. Stein, Y. Liu, W. G. Yin, and C. Petrovic, Magnetotransport properties of MoP_2 , *Phys. Rev. B* **96**, 195107 (2017).
- [43] A. F. Wang, D. Graf, Y. Liu, Q. H. Du, J. B. Zheng, H. C. Lei, and C. Petrovic, Large magnetoresistance in the type-II Weyl semimetal WP_2 , *Phys. Rev. B* **96**, 121107(R) (2017).
- [44] N. H. Jo, Y. Wu, L.-L. Wang, P. P. Orth, S. S. Downing, S. Manni, D. Mou, D. D. Johnson, A. Kaminski, S. L. Bud'ko, and P. C. Canfield, Extremely large magnetoresistance and Kohler's rule in PdSn_4 : A complete study of thermodynamic, transport, and band-structure properties, *Phys. Rev. B* **96**, 165145 (2017).
- [45] Y. K. Luo, H. Li, Y. M. Dai, H. Miao, Y. G. Shi, H. Ding, A. J. Taylor, D. A. Yarotski, R. P. Prasankumar, and J. D. Thompson, Hall effect in the extremely large magnetoresistance semimetal WTe_2 , *Appl. Phys. Lett.* **107**, 182411 (2015).
- [46] D. Shoenberg, *Magnetic Oscillation in Metals* (Cambridge University Press, Cambridge, 1984).